Interval Sliding Mode Observer Based Incipient Sensor Fault Detection with Application to a Traction Device in China Railway High-speed

Kangkang Zhang, Bin Jiang, *Senior Member, IEEE*, Xianggang Yan and Jun Shen

***Abstract*—This paper proposes an interval sliding mode observer (ISMO) and an incipient sensor faults detection method for a class of nonlinear control systems with observer unmatched uncertainties. The interval bounds for continuous nonlinear functions and new injection functions are constructed to design ISMOs. An incipient fault detection framework with newly designed residual and threshold generators is proposed. The detectability is then studied, and a set of sufficient detectable conditions are presented. Applications to an electrical traction device used in China Railway High-speed (CRH) are presented to verify the effectiveness of the proposed incipient sensor fault detection methodology.**

***Index Terms*—Interval observer, sliding mode, incipient fault detection, traction device.**

I. Introduction

Fault tolerant control and fault diagnosis techniques have been given greater concerns and widely studied [1]- [14]. Observer-based fault diagnosis is one powerful techniques in the field of model-based diagnosis, in which analytical redundancy is first established through the diagnostic observer to reconstruct measured outputs. Then, the residuals used to diagnose faults are generated by comparing the system measurable outputs with the corresponding redundancy. In ideal case, the residuals are zero in fault-free scenario. Unfortunately, the residuals are usually not zero due to modeling error and possible uncertainties experienced by the systems. Thus, the threshold concept is introduced to distinguish the faults from uncertainties through residuals. It is an efficient idea for general serious abrupt faults detection because abrupt faults always have larger effects on residuals than uncertainties [4]. However, this idea may not be pertinent to incipient fault diagnosis because the influence of incipient faults on residuals is easily submerged by uncertainties. This is great challenging for observer-based incipient fault detection (IFD), particularly for incipient sensor fault detection (ISFD).

Observer-based fault diagnosis for nonlinear control systems has been studied extensively such as [7], [8], [9] and [14]. High accuracy output reconstruction is one of the main tasks of the diagnostic observer in observer-based fault diagnosis, which is particularly important for IFD. However, it is impossible to reconstruct the outputs precisely only by input-output signals using Luenberger observer for nonlinear systems because observer unmatched uncertainties can not be eliminated from the output channels. Nevertheless, the interval estimation technique is proposed in [15] for the first time and is used to estimate the lower and upper bounds of uncertain dynamic systems with uncertainties propagated by interval models. Interval observers have no structural limitation on uncertainties, which improves the robustness against modeling uncertainties and disturbances effectively, which have been used in fault diagnosis fields such as [16] and [17]. Therefore, to use the interval observers as diagnostic observer provides a new idea for IFD. However, until now, most existing interval observers are for linear systems [15] or LPV systems [16] and [18], nonlinear functions in these papers are usually replaced by an enlarged parametric variation in the LPV representation. An interval observer design scheme is proposed for Lipschitz nonlinear systems in [19], which motivates the study of nonlinear complexity by relaxing Lipschitz condition.

Over the past few decades, sliding mode observer based fault diagnosis has also been studies and used widely (see e.g., [20] and [21]). The sliding mode observer is used to diagnose faults for the first time in [21] which considers the disruption of sliding motion and has motivated the research in this area. The “equivalent output injection" concept is used to reconstruct sensor and actuator faults signals and then detect and isolate then explicitly in [20]. In [22], another FDI (fault detection and isolation) method is developed by using sliding mode observer to generate residuals instead of reconstructing fault signals. All results above require that the system detectable and the observer matched structural condition is satisfied. Therefore, interval estimation with sliding mode technique is a pertinent solution to ISFD.

Recently, an ISMO is proposed in [23] to detect incipient sensor faults. Built on the author's previous work in [23], ISFD schemes with detailed analysis and solid results are developed for a class of nonlinear control systems in this paper. The Min-Max approach [24] is employed in this paper to obtain the interval model for a class of nonlinear functions. Then, the

This work is supported in part by the National Natural Science Foundation of China (Grant 61490703, 61573180 and 61603180), Priority Academic Program Development of Jiangsu Higher Education Institutions, Fundamental Research Funds for the Central Universities (NO. NE2014202), the Natural Science Foundation of Jiangsu Province (BK20160810), and the Fundamental Research Funds for the Central Universities (90YAH16011).

Kangkang Zhang, Bin Jiang and Jun Shen are with the College of Automation Engineering, Nanjing University of Aeronautics and Astronautics, and Jiangsu Key Laboratory of Internet of Things and Control Technologies, Nanjing210016, China, email: kangzhang359@nuaa.edu.cn; binjiang@nuaa.edu.cn; junshen2009@gmail.com.

Xinggang Yan is with School of Engineering and Digital Arts, University of Kent, Canterbury, Kent CT2 7NT, United Kingdom, email: x.yan@kent.ac.uk.

* Corresponding author: Bin Jiang.

ISFD framework is established with new proposed residual generator and corresponding threshold generator. Moreover, the detectability is studied, and sufficient conditions on incipient faults are obtained. In this paper, the main contribution is summarized as follows:

(i) an ISMO is proposed as diagnostic observer for a class of nonlinear control systems with observer unmatched uncertainties,
(ii) an ISFD framework is established with new residual generator and threshold generator.

The rest parts are organized as follows. In Section II, problem formulation and preliminaries are presented. In Section III, the ISMO is designed as the diagnostic observer. In Section IV, the residual and corresponding threshold generators are proposed. In Section V, Verification in the TDCS-FIB is presented. Section VI concludes this paper.

Notation: In this paper, $\|\cdot\|$ represents the 2−norm. For a matrix or vector M, all elements of M are positive (nonnegative) is denoted by $M > 0$ ($M \geq 0$). For two vectors $x_1,\ x_2 \in \mathcal{R}^n$ or matrices $A_1,\ A_2 \in \mathcal{R}^{n\times n}$, $x_1 \leq x_2$ and $A_1 \leq A_2$ are defined in element wise, respectively. For a matrix $A \in \mathcal{R}^{m\times n}$, $A^+ = \max\{0, A\}$ and $A^- = A^+ - A$. It should be noted that A^+ and A^- are nonnegative.

II. Preliminaries and Problem Formulations

The following two lemmas are firstly introduced.

Lemma 1: [18] Let $x,\ \underline{x},\ \bar{x} \in \mathcal{R}^n$ satisfy that $\underline{x} \leq x \leq \bar{x}$. Then for matrices A with appropriate dimensions, $A^+\underline{x} - A^-\bar{x} \leq Ax \leq A^+\bar{x} - A^-\underline{x}$.

Lemma 2: For any $\hat{x} \in \Sigma$ with $\Sigma \subseteq \mathcal{R}^h$ being a closed compact set, and for any continuous scalar function $g(x, y, u)$ with $x \in \Sigma$, there exist $w(\hat{x}, y, u) \in \mathcal{R}^h$ and $a(\hat{x}, y, u) \in \mathcal{R}$ such that

$$J(w(\cdot), x) - a(\cdot) \leq 0 \tag{1}$$

where $J(w, x) = \operatorname{sgn}(\alpha)\left(\mathrm{g}(x, y, u) - \mathrm{g}(\hat{x}, y, u) + w(\cdot)(x - \hat{x})\right)$ with α being a known scalar.

Proof: : See [24] and [25]. ■

Remark 1: An available way to obtain $w(\cdot)$ and $a(\cdot)$ is to solve the optimization problem

$$a(\cdot) = \min_{w\in\mathcal{R}^h} \max_{x\in\Sigma} J(w, x), w(\cdot) = \arg\min_{w\in\mathcal{R}^h} \max_{x\in\Sigma} J(w, x). \tag{2}$$

which is presented in [24] and [25]. ∇

Remark 2: Lemma 1 is usually used in interval observer design. Lemma 2 provides a way to obtain the interval model of general continuous functions. Reference [19] presents a method to design interval observers for global Lipschitz systems, this paper proposes a way to design for general continuous systems. ∇

Generally speaking, incipient faults have small amplitude, and develop continuously and slowly. Based on [28], the incipient sensor fault $f \in \mathcal{R}^q$ considered in this paper is modeled by

$$\dot{f} = A_f f + \xi(t) \tag{3}$$

where $A_f \in \mathcal{R}^{q\times q}$ is the Hurwitz matrix, and $\xi(t) \in \mathcal{R}^q$ is a driving signal. It should be pointed out that for an incipient fault f and a given Hurwitz matrix A_f, there always exist driving signal $\xi(t)$ satisfying (3).

Consider nonlinear systems with incipient sensor faults modeled by (3)

$$\dot{z} = A_z z + g_z(z, y, u) + B_z u + \eta_z(z, u, \omega, t), \tag{4}$$
$$y = C_z z + [0_{(p-q)\times q}, I_q]^\top f \tag{5}$$

where $z \in \mathcal{R}^{n_0}$ is state, $u \in \mathcal{R}^m$ is control, $y \in \mathcal{R}^p$ is output. The function $g_z(\cdot)$ is a known nonlinear continuous vector field, and $\eta_z(\cdot)$ represents lumped uncertainties which includes perturbation parameters, unmodeled dynamics, system uncertainties and external and internal disturbances (noises) [29]. It is assumed throughout the paper that $p \geq q$.

Using the augmentation method presented in [4], the nonlinear system (4)-(5) and incipient sensor fault (3) can be augmented with inherent relative degree one. Then, based on [20], there exists a coordinate transformation such that the augmented system is transformed to

$$\dot{x}_1 = A_{11}x_1 + A_{12}x_2 + g_1(x_1, y, u) + B_1 u + \eta_1(\cdot), \tag{6}$$
$$\dot{x}_{21} = A_{211}x_1 + A_{22}^{11}x_{21} + A_{22}^{12}x_{22} + g_{21}(\cdot) + B_{21}u + \eta_{21}(\cdot), \tag{7}$$
$$\dot{x}_{22} = A_{212}x_1 + A_{22}^{21}x_{21} + A_{22}^{22}x_{22} + g_{22}(\cdot) + B_{22}u + \eta_{22}(\cdot) + \xi(\cdot), \tag{8}$$
$$y = C_{21}x_{21} + C_{22}x_{22} \tag{9}$$

where $x_1 \in \mathcal{R}^{n_1}$ and $x_{21} \in \mathcal{R}^{p-q}$ and $x_{22} \in \mathcal{R}^q$ with $n_1 + p = n_0 + q = n$. The uncertainty $\eta_1(\cdot)$ is observer unmatched which is challenging to deal with. The matrix $C_2 = [C_{21}, C_{22}]$ is nonsingular. It is assumed throughout this paper that all the nonlinear vectors $g_1(\cdot)$, $g_{21}(\cdot)$ and $g_{22}(\cdot)$ satisfy the conditions in Lemma 2. For a practical system, there always exists an inherent interval $\Omega = [x_{1\min},\ x_{1\max}]$ such that no matter when faults occur, $x_1 \in \Omega$.

Assumption 1: There exist functions $\bar{\eta}_{21}(y, u, t)$, $\underline{\eta}_1(y, u, t)$, $\bar{\eta}_1(y, u, t)$, $\underline{\eta}_{22}(y, u, t)$ and $\bar{\eta}_{22}(y, u, t)$ such that $\|\eta_{21}(\cdot)\| \leq \bar{\eta}_{21}(\cdot)$, $\underline{\eta}_1(\cdot) \leq \eta_1(\cdot) \leq \bar{\eta}_1(\cdot)$ and $\underline{\eta}_{22}(\cdot) \leq \eta_{22}(\cdot) \leq \bar{\eta}_{22}(\cdot)$. Moreover, there exist $\underline{\Delta}_{\eta_1}$, $\bar{\Delta}_{\eta_1}$, $\underline{\Delta}_{\eta_{22}}$ and $\bar{\Delta}_{\eta_{22}}$ such that $\eta_1(\cdot) - \underline{\eta}_1(\cdot) \leq \underline{\Delta}_{\eta_1}$, $\bar{\eta}_1(\cdot) - \eta_1(\cdot) \leq \bar{\Delta}_{\eta_1}$, $\eta_{22}(\cdot) - \underline{\eta}_{22}(\cdot) \leq \underline{\Delta}_{\eta_{22}}$ and $\bar{\eta}_{22}(\cdot) - \eta_{22}(\cdot) \leq \bar{\Delta}_{\eta_{22}}$.

Remark 3: The function $\bar{\eta}_{21}(\cdot)$ in Assumption 1 usually appears in sliding mode observer design papers such as [20] and [30] and it is quite reasonable to assume $\eta_{21}(\cdot)$ is norm bounded. Also, Assumption 1 provides interval models of disturbances for subsystems (6) and (8). ∇

III. Interval Sliding Mode Diagnostic Observer Design

The *Appendix A* provides an interval model $[\bar{\varphi}_1(\bar{x}_1, \underline{x}_1, \cdot), \underline{\varphi}_1(\bar{x}_1, \underline{x}_1, \cdot)]$ in (*A*.2) for the nonlinearity $g_1(\cdot)$. Based on the interval model, the dynamics of $\bar{x}_1$ and $\underline{x}_1$ are proposed by

$$\dot{\bar{x}}_1 = A_{11}\bar{x}_1 + A_{12}C_2^{-1}y + \bar{\varphi}_1\left(\bar{x}_1, \underline{x}_1, \cdot\right) + \bar{\eta}_1(\cdot) + B_1 u + F_1(\bar{x}_1 - \underline{x}_1), \tag{10}$$
$$\dot{\underline{x}}_1 = A_{11}\underline{x}_1 + A_{12}C_2^{-1}y + \underline{\varphi}_1\left(\bar{x}_1, \underline{x}_1, \cdot\right) + \underline{\eta}_1(\cdot) + B_1 u - F_1(\bar{x}_1 - \underline{x}_1) \tag{11}$$

$$\tilde{A}_{11} = \left[\begin{array}{c|c} A_{11} + F_1 + \left(\underline{\mathbb{W}}_1^- + \bar{\mathbb{W}}_1^+\right)(\bar{x}_1, \cdot) & F_1 + \bar{\mathbb{W}}_1^+(\bar{x}_1, \cdot) \\ \hline F_1 + \bar{\mathbb{W}}_1^+(\underline{x}_1, \cdot) & A_{11} + F_1 + (\bar{\mathbb{W}}_1^- + \bar{\mathbb{W}}_1^+)(\underline{x}_1, \cdot) \end{array}\right].$$

where the gain matrix $F_1 \in \mathcal{R}^{n_1 \times n_1}$ is nonnegative which will be determined later. The initial states satisfy $\underline{x}_1(0),\ \bar{x}_1(0) \in \Omega$ and $\underline{x}_1(0) \le x_1(0) \le \bar{x}_1(0)$.

Denote $e_1 = [\bar{e}_1, \underline{e}_1]^\top$ where $\bar{e}_1 = \bar{x}_1 - x_1$ and $\underline{e}_1 = x_1 - \underline{x}_1$. By comparing (10) and (11) with (6), the error dynamic is obtained by

$$\dot{e}_1 = \hat{A}_{11} e_1 + \phi(\bar{x}_1, \underline{x}_1, x_1, \cdot) \tag{12}$$

where

$$\hat{A}_{11} = \left[\begin{array}{c|c} A_{11} + F_1 & F_1 \\ \hline F_1 & A_{11} + F_1 \end{array}\right]$$

and

$$\phi(\cdot) = \left[\begin{array}{c} \bar{\varphi}_1(\cdot) - g_1(\cdot) + \bar{\eta}_1(\cdot) - \eta_1(\cdot) \\ g_1(\cdot) - \underline{\varphi}_1(\cdot) + \eta_1(\cdot) - \underline{\eta}_1(\cdot) \end{array}\right].$$

From (*A*.5), (*A*.6) and Assumption 1, it follows that

$$\phi(\cdot) \le \left[\begin{array}{c} \left(\underline{\mathbb{W}}_1^- + \bar{\mathbb{W}}_1^+\right)(\bar{x}_1, \cdot)\bar{e}_1 + \bar{\mathbb{W}}_1^+(\bar{x}_1, \cdot)\underline{e}_1 \\ (\bar{\mathbb{W}}_1^- + \bar{\mathbb{W}}_1^+)(\underline{x}_1, \cdot)\underline{e}_1 + \bar{\mathbb{W}}_1^+(\underline{x}_1, \cdot)\bar{e}_1 \end{array}\right] + \tilde{\phi}$$

where $\tilde{\phi} \ge 0$ and

$$\tilde{\phi} = \left[\begin{array}{c} (\underline{\mathbb{A}}_1 + \bar{\mathbb{A}}_1)(\bar{x}_1, \cdot) + \bar{\Delta}_{\eta_1}(\cdot) \\ (\underline{\mathbb{A}}_1 + \bar{\mathbb{A}}_1)(\underline{x}_1, \cdot) + \underline{\Delta}_{\eta_1}(\cdot) \end{array}\right].$$

Then (12) becomes

$$\dot{e}_1 \le \tilde{A}_{11} e_1 + \tilde{\phi} \tag{13}$$

where $\tilde{A}_{11}$ is given in the top of this page.

Based on system (13), a system is constructed as follows

$$\dot{v} = \bar{A}_{11} v + \tilde{\phi},\ v(0) \ge e_1(0) \tag{14}$$

where $\bar{A}_{11} \ge \tilde{A}_{11}$. Then a proposition is ready to be presented.

Proposition 1: Under Assumption 1, if there exists a nonnegative matrix F_1 such that

- both the matrices $\hat{A}_{11}$ and $\tilde{A}_{11}$ are the Metzler matrices,
- there exist the Metzler and Hurwitz matrix $\bar{A}_{11}$ such that

$$\bar{A}_{11} \ge \tilde{A}_{11}, \tag{15}$$

then $0 \le e_1 \le v$ and (10)-(11) is an interval observer of subsystem (6).

Proof: From $\underline{x}_1(0) \le x_1(0) \le \bar{x}_1(0)$, it is straightforward to see that $e_1(0) \ge 0$. Consider the first time constant t_1 when one of the components of vector e_1 in (12) is equal to zero. Suppose that it is $\bar{e}_{1i}$. Then

$$\dot{\bar{e}}_{1i}(t_1) = \sum_{j=1, j\ne i}^{n_1} (A_{11ij} + F_{1ij})\bar{e}_{1j}(t_1) + \sum_{j=1}^{n_1} F_{1ij}\underline{e}_{1j}(t_1) + \phi_i(\cdot)|_{t=t_1}$$

where A_{11ij} and F_{1ij} represent the elements of the ith row and jth column of A_{11} and F_1, respectively. From the interval bounds in (*A*.2) and Assumption 1, $\phi_i(\cdot)|_{t=t_1} \ge 0$. Because the matrix $\hat{A}_{11}$ is Metzler, and F_1 is positive, $A_{11ij} + F_{1ij} > 0$ for $\forall i \ne j$. Then $\dot{\bar{e}}_{1i}(t_1) > 0$, which implies that $\bar{e}_{1i}(t) > 0$ for $t > t_1$. Thus, it can be concluded that $\bar{e}_{1i}$ remains positive for $t \ge 0$. Using the same analysis on $\underline{e}_{1i}$, it is easy to obtain that $\underline{e}_{1i} > 0$ for $t \ge 0$ as well. Therefore, $e_{1i}(t) \ge 0$ for $t \ge 0$.

Moreover, since $\bar{A}_{11} \ge \tilde{A}_{11}$ and $e_1 \ge 0$, $\tilde{A}_{11}e_1 \le \bar{A}_{11}e_1$ and then $\dot{e}_1 \le \bar{A}_{11}e_1 + \tilde{\phi}$. Using the Comparing Principle presented in [31], if the initial condition satisfies $0 \le e_1(0) \le v(0)$, then $0 \le e_1 \le v$ where v is the state of the constructed system (14). Since $\bar{A}_{11}$ is the Hurwitz and Metzler matrix, $v \ge 0$ and asymptotically converges to an interval with its upper bound being associated with $\bar{A}_{11}$ and $\tilde{\phi}$. Thus, e_1 also asymptotically converges to this interval.

Hence, the result follows. ■

Remark 4: Many different interval observers have been proposed (see [26]) for systems with different uncertain structures and [27] has provided a method to design interval observers for linear systems with uncertain structural parameters. Unfortunately, due to the time-varying and state-related characteristic of $\tilde{A}_{11}$, the stability condition to guarantee the convergence of the interval observer in [27] cannot be applied. On the other hand, it is still challenging to ensure the stability of systems with time-varying and state-related system matrix $\tilde{A}_{11}$. In this paper, the Metzler and Hurwitz matrix $\bar{A}_{11}$ is introduced to deal with this issue. ∇

Denote $\bar{v} = \text{diag}\{I_{n_1}, 0\}v$ and $\underline{v} = \text{diag}\{0, I_{n_1}\}v$. From $0 \le e_1 \le v$ in Proposition 1,

$$0 < \bar{e}_1 \le \bar{v},\ 0 < \underline{e}_1 \le \underline{v} \tag{16}$$

which will be used in the following sections.

From Proposition 1, the sub-observer (10)-(11) provides estimates of upper and lower bounds of x_1 respectively. Then $\hat{x}_1$, the estimate of x_1, can be constructed by using midpoint of the interval $[\underline{x}_1, \bar{x}_1]$, i.e.

$$\hat{x}_1 = \frac{\underline{x}_1 + \bar{x}_1}{2}. \tag{17}$$

Then the estimate error is obtained by

$$\mathbb{e}_1 = x_1 - \hat{x}_1 = \frac{\underline{e}_1 - \bar{e}_1}{2}. \tag{18}$$

From Proposition 1 that $0 \le e_1 \le v$, it yields

$$\|\mathbb{e}_1\| \le \frac{1}{2}(\|\bar{e}_1\| + \|\underline{e}_1\|) \le \|v\|. \tag{19}$$

Denote $\hat{x}_{21}$ as estimate of x_{21}. For sub-system (7), consider the following sub-observer

$$\begin{aligned} \dot{\hat{x}}_{21} =& A_{211}\hat{x}_1 + A_{22}^{11}\hat{x}_{21} + A_{22}^{12}x_{22} + g_{21}(\hat{x}_1, \cdot) \\ &+ (A_{22}^{11} - \hat{A}_{22}^{11})(x_{21} - \hat{x}_{21}) + B_{21}u + \nu_1 + \nu_2 \end{aligned} \tag{20}$$

where $\hat{A}_{22}^{11}$ is symmetric negative definite, and functions ν_1 and ν_2 are given by

$$\nu_1 = m_1(\cdot)\text{sign}(x_{21} - \hat{x}_{21}), \tag{21}$$

$$\nu_2 = M_2(\cdot)\text{sign}(x_{21} - \hat{x}_{21}) \tag{22}$$

where $m_1(\cdot)$ is a positive scalar function, and $M_2(\cdot)$ is a diagonal matrix function, which are both determined later.

Remark 5: The choice $\hat{x}_1$ in (17) is used to ensure that $\mathbb{e}_1$ can be bounded by assured upper and low bounds, which are required to design gains $m_1(\cdot)$ and $M_2(\cdot)$. ∇

Denote $e_{21} = x_{21} - \hat{x}_{21}$. Based on Lemma 2, for $g_{21i}(x_1, \cdot)$, the ith component of $g_{21}(x_1, \cdot)$, there exist vector $w_{21i}(\hat{x}_1, \cdot)$ and a scalar $a_{21i}(\hat{x}_1, \cdot)$, $i = 1, 2, \cdots, p-q$ such that

$$\Pi_i = \text{sign}(e_{21i})(g_{21i}(x_1, \cdot) - g_{21i}(\hat{x}_1, \cdot) + w_{21i}(\cdot)\mathbb{e}_1) - a_{21i}(\cdot) \leq 0. \tag{23}$$

Denote $\mathbb{W}_{21}(\cdot) = \text{diag}\{w_{211}\}$. By comparing (20) with (7), the error dynamic is obtained by

$$\begin{aligned}\dot{e}_{21} =&(A_{211} - \mathbb{W}_{21}(\cdot))\mathbb{e}_1 + \hat{A}_{22}^{11}e_{21} + g_{21}(x_1, \cdot) - g_{21}(\hat{x}_1, \cdot)\\ &+ \mathbb{W}_{21}(\cdot)\mathbb{e}_1 + \eta_{21}(\cdot) - \nu_1 - \nu_2.\end{aligned} \tag{24}$$

Consider a hyperplane

$$\mathscr{L} = \{(\mathbb{e}_1, e_{21}) | e_{21} = 0\}. \tag{25}$$

Then, the following conclusion is ready to be presented.

Proposition 2: Under Assumption 1, error system (24) is driven to the sliding surface $\mathscr{L}$ given by (25) in finite time and maintains on it thereafter if the gains $m_1(y, u, t)$ and $M_2(\hat{x}_1, \cdot)$ in (21) and (22) satisfy that

$$m_1(\cdot) \geq \|A_{211} - \mathbb{W}_{21}(\cdot)\|w + \bar{\eta}_{21}(y, u, t) + \kappa, \tag{26}$$

$$M_2(\cdot) = \text{diag}\{a_{21i}\} \tag{27}$$

where κ is a positive constant scalar.

Proof: Let $V = \frac{1}{2}e_{21}^T e_{21}$ be the Lyapunov function candidate. It follows from the error dynamic (24) that

$$\begin{aligned}\dot{V} =&\frac{1}{2}e_{21}^T\left(\hat{A}_{22}^{11} + \hat{A}_{22}^{11T}\right)e_{21}\\ &+ e_{21}^T\left((A_{211} - \mathbb{W}_{21}(\cdot))\mathbb{e}_1 + \eta_{21}(\cdot) - \nu_1\right)\\ &+ e_{21}^T(g_{21}(x_1, \cdot) - g_{21}(\hat{x}_1, \cdot) + \mathbb{W}_{21}(\cdot)\mathbb{e}_1 - \nu_2).\end{aligned}$$

Since $\hat{A}_{22}^{11}$ is symmetric negative definite, $e_{21}^T(\hat{A}_{22}^{11} + \hat{A}_{22}^{11^T})e_{21} \leq 0$. Then,

$$\begin{aligned}\dot{V} \leq& \|e_{21}\|\left(\|(A_{211} - \mathbb{W}_{21}(\cdot))\|\,\|\mathbb{e}_1\| + \|\eta_{21}(\cdot)\|\right) - m_1(\cdot)\|e_{21}\|\\ &+ e_{21}^T(g_{21}(x_1, \cdot) - g_{21}(\hat{x}_1, \cdot) + \mathbb{W}_{21}(\cdot)\mathbb{e}_1 - M_2(\cdot)\text{sgn}(e_{21})).\end{aligned}$$

Note that it follows from (23) that

$$\begin{aligned}&e_{21}^T\left((g_{21}(x_1, \cdot) - g_{21}(\hat{x}_1, \cdot) + \mathbb{W}_{21}(\cdot)\mathbb{e}_1) - M_2(\cdot)\text{sign}(e_{21})\right)\\ &= \sum_{i=1}^{p-q} e_{21i}\left((g_{2i}(x_1, \cdot) - g_{2i}(\hat{x}_1, \cdot) + w_{2i}(\cdot)\mathbb{e}_1) - a_{2i}(\cdot)\text{sign}(e_{21i})\right)\\ &= \sum_{i=1}^{p-q} |e_{21i}|\,\Pi_i \leq 0.\end{aligned} \tag{28}$$

Thus, it can be concluded that $\dot{V} \leq -\kappa\|e_{21}\| \leq -\kappa V^{1/2}$, which means that the "$\eta$−reachability condition" is satisfied.

Hence, the conclusion follows. ■

From subsystem (8), it can be seen that the fault related term $\xi(\cdot)$ affects x_{22} directly, which implies that only using x_{22} is sufficient to detect incipient faults. Thus, in sub-observer design for (8), the residual generation and threshold generation problems should be pre-considered. The sub-observer for (8) is proposed by

$$\begin{aligned}\dot{\bar{x}}_{22} =&A_{212}\bar{x}_1 + A_{22}^{21}\hat{x}_{21} + A_{22}^{22}\bar{x}_{22} + g_{22}(\bar{x}_1, \cdot) + B_{22}u\\ &+ F_2(\bar{x}_1 - \underline{x}_1) + K_{22}\left(x_{22} - \bar{x}_{22}\right), \bar{x}_{22}(0) = x_{22}(0),\end{aligned} \tag{29}$$

$$\begin{aligned}\dot{\underline{x}}_{22} =&A_{212}\underline{x}_1 + A_{22}^{21}\hat{x}_{21} + A_{22}^{22}\underline{x}_{22} + g_{22}(\underline{x}_1, \cdot) + B_{22}u\\ &- F_2(\bar{x}_1 - \underline{x}_1) + K_{22}\left(x_{22} - \underline{x}_{22}\right), \underline{x}_{22}(0) = x_{22}(0)\end{aligned} \tag{30}$$

where the gain matrix K_{22} is chosen as $A_{22}^{22} - \hat{A}_{22}^{22}$ with $\hat{A}_{22}^{22}$ being the Hurwitz and Metzler matrix. The gain F_2 is a nonnegative matrix to be chosen to ensure that $A_{212} + F_2$ is also nonnegative.

Therefore, the design of diagnostic observer characterized by sub-observers (10)-(11), (20) and (29)-(30) is completed. In next section, incipient sensor fault detection schemes will be presented.

IV. Incipient Fault Detection Schemes

A. Residual Generation

The residual r is defined as $r = [\bar{x}_{22} - x_{22}, x_{22} - \underline{x}_{22}]^\top$. Then by comparing (29) and (30) with (8), the residual generator $\dot{r}$ is obtained by

$$\begin{aligned}\dot{r} =&\left[\begin{array}{c|c} A_{212} + F_2 & F_2 \\ \hline F_2 & A_{212} + F_2 \end{array}\right]\left[\begin{array}{c} \bar{e}_1 \\ \underline{e}_1 \end{array}\right] + \left[\begin{array}{c} A_{22}^{21} \\ A_{22}^{21} \end{array}\right]e_{21}\\ &+ \left[\begin{array}{cc} \hat{A}_{22}^{22} & 0 \\ 0 & \hat{A}_{22}^{22} \end{array}\right]r + \left[\begin{array}{c} g_{22}(\bar{x}_1, \cdot) - g_{22}(x_1, \cdot) \\ g_{22}(x_1, \cdot) - g_{22}(\underline{x}_1, \cdot) \end{array}\right]\\ &+ \left[\begin{array}{c} -\xi(\cdot) \\ \xi(\cdot) \end{array}\right] + \left[\begin{array}{c} -\eta_{22}(\cdot) \\ +\eta_{22}(\cdot) \end{array}\right]\end{aligned} \tag{31}$$

where the initial value of r is chosen as $r(0) = 0$.

Remark 6: After sliding motion takes place, $e_{21} = 0$ which means that r does not rely on the estimate of $\hat{x}_{21}$ during the sliding motion. ∇

B. Adaptive Threshold Generation

Adaptive thresholds should be higher than residuals in fault free scenario. As the residual r is used directly to detect incipient faults without evaluation, the threshold is chosen as its upper bound.

Based on Lemma 2, there exist $\underline{\mathbb{W}}_{22}(\bar{x}_1, \cdot) = \text{diag}\{\underline{w}_{22i}\}$, $\underline{\mathbb{A}}_{22}(\bar{x}_1, \cdot) = [\underline{a}_{22i}]^\top$, $\bar{\mathbb{W}}_{22}(\underline{x}_1, \cdot) = \text{diag}\{\bar{w}_{22i}\}$ and $\bar{\mathbb{A}}_{22}(\underline{x}_1, \cdot) = [\bar{a}_{22i}]^\top$ such that

$$g_{22}(\bar{x}_1, \cdot) - g_{22}(x_1, \cdot) \leq \underline{\mathbb{A}}_{22}(\bar{x}_1, \cdot) - \underline{\mathbb{W}}_{22}(\bar{x}_1, \cdot)\bar{e}_1, \tag{32}$$

$$g_{22}(x_1, \cdot) - g_{22}(\underline{x}_1, \cdot) \leq \bar{\mathbb{A}}_{22}(\underline{x}_1, \cdot) - \bar{\mathbb{W}}_{22}(\underline{x}_1, \cdot)\underline{e}_1. \tag{33}$$

Note that $\underline{\mathbb{W}}_{22}(\cdot) = \underline{\mathbb{W}}_{22}^+(\cdot) - \underline{\mathbb{W}}_{22}^-(\cdot)$ with $\underline{\mathbb{W}}_{22}^+(\cdot)$ and $\underline{\mathbb{W}}_{22}^-(\cdot)$ being nonnegative. From Proposition 1 and (16), $-\underline{\mathbb{W}}_{22}(\cdot)\bar{e}_1 \leq \underline{\mathbb{W}}_{22}^-(\cdot)\bar{v}$. Similarly, $-\underline{\mathbb{W}}_{22}(\cdot)\underline{e}_1 \leq \bar{\mathbb{W}}_{22}^-(\cdot)\underline{v}$. In addition, due to the negativity of $A_{212} + F_2$ and F_2, $(A_{212} + F_2)\bar{e}_1 \leq (A_{212} + F_2)\bar{v}$, $(A_{212} + F_2)\underline{e}_1 \leq (A_{212} + F_2)\underline{v}$, $F_2\bar{e}_1 \leq F_2\bar{v}$ and $F_2\underline{e}_1 \leq F_2\underline{v}$.

After sliding motion takes place, $e_{21} = \dot{e}_{21} = 0$. Based on (31), the threshold generator $\dot{J}_{th}$ is constructed as follows

$$\begin{aligned}\dot{J}_{th} =&\left[\begin{array}{c|c} A_{212} + F_2 & F_2 \\ \hline F_2 & A_{212} + F_2 \end{array}\right]\left[\begin{array}{c} \bar{v} \\ \underline{v} \end{array}\right] + \left[\begin{array}{cc} \hat{A}_{22}^{22} & 02 \\ 0 & \hat{A}_{22}^{22} \end{array}\right]J_{th}\\ &+ \left[\begin{array}{c} \underline{\mathbb{W}}_{22}^-(\bar{x}_1, \cdot)\bar{v} + \underline{\mathbb{A}}_{22}(\bar{x}_1, \cdot) \\ \bar{\mathbb{W}}_{22}^-(\underline{x}_1, \cdot)\underline{v} + \bar{\mathbb{A}}_{22}(\underline{x}_1, \cdot) \end{array}\right] + \left[\begin{array}{c} -\underline{\eta}_{22}(\cdot) \\ +\bar{\eta}_{22}(\cdot) \end{array}\right]\end{aligned} \tag{34}$$

where the initial value of J_{th} is chosen as $J_{th}(0) = 0$. Comparing with (31), due to Metzler matrix $\hat{A}_{22}^{22}$, in fault free scenario (i.e. $\xi(\cdot) = 0$), $r \leq J_{th}$. Therefore, J_{th} is chosen as adaptive threshold.

Remark 7: It should be pointed out that r and J_{th} satisfy $r < J_{th}$ only on the sliding surface (25). It usually takes longer time for incipient faults (for example, mechanical wear) to cause serious system failure. Moreover, the reaching time of sliding motion can be shortened by choosing a big reachability constant. Therefore, the developed results can be applied to a majority of cases in reality. ∇

C. Incipient Fault Detection Decision

Firstly, denote detection index $\Gamma = 1$ as that fault is detected and $\Gamma = 0$ as that fault is not detected. In this paper, **the decision on occurrence of incipient sensor faults is made** if during sliding motion, there exists at least one j, $j = 1, \cdots, 2q$ such that $r_j(T_d)$ exceeds the corresponding adaptive threshold $J_{thj}(T_d)$ and remains that thereafter where T_d is the fault detection time, that is

- $r_j(T_d) > J_{thj}(T_d)$, $\Gamma_j = 1$,
- otherwise, $\Gamma_j = 0$.

Accordingly, the detection time T_d is defined as the first time when $r_j(T_d) > J_{thj}(T_d)$ and remains that thereafter for some $j = 1, \cdots, 2q$, i.e.,

$$T_d \triangleq \inf \bigcup_{j=1}^{2q} \left\{ t > 0 \,\middle|\, r_j(t) > J_{thj}(t) \right\}. \tag{35}$$

D. Incipient Fault Detectability

Denote $\Delta_r = J_{th} - r$. As analyzed above, in fault-free scenario (i.e. $\xi(\cdot) = 0$), $\Delta_r \geq 0$, and in fault case, the incipient sensor fault is detected if there exists a j, $j = 1, \cdots, 2p$ such that $\Delta_{rj} < 0$ where Δ_{rj} is the jth row of Δ_r. Comparing (31) with adaptive threshold (34), the dynamics of Δ_r can be obtained. Due to inequalities (32)-(33),

$$\dot{\Delta}_r \geq A_\Delta \Delta_r + D_\Delta(v - e_1) + \Delta_{\eta_{22}} - \Delta_{\xi(\cdot)} \tag{36}$$

where

$$D_\Delta = \left[\begin{array}{c|c} A_{212} + F_2 + \underline{\mathbb{W}}_{22}^{-}(\bar{x}_1, \cdot) & F_2 \\ \hline F_2 & A_{212} + F_2 + \bar{\mathbb{W}}_{22}^{-}(\bar{x}_1, \cdot) \end{array} \right],$$

$$A_\Delta = \begin{bmatrix} \hat{A}_{22}^{22} & 0 \\ 0 & \hat{A}_{22}^{22} \end{bmatrix}, \ \Delta_{\eta_{22}} = \begin{bmatrix} \underline{\Delta}_{\eta_{22}} \\ \bar{\Delta}_{\eta_{22}} \end{bmatrix}, \ \Delta_{\xi(\cdot)} = \begin{bmatrix} \xi(\cdot) \\ -\xi(\cdot) \end{bmatrix}$$

with $\underline{\Delta}_{\eta_{22}} = \eta_{22} - \underline{\eta_{22}}$ and $\bar{\Delta}_{\eta_{22}} = \bar{\eta}_{22} - \eta_{22}$.

Now, Choose $\hat{A}_{22}^{22} = -\alpha I_q$ with $\alpha > 0$. By integrating (36) in both sides from T_0 (T_0 is the fault occurrence time instant) to T_d, each component of Δ_r, Δ_{rj} satisfies that

$$\begin{aligned} \Delta_{rj}(T_d) \geq & \Delta_{rj}(T_0) + \int_{T_0}^{T_d} e^{-\alpha(t-\tau)} [D_\Delta(v - e_1) + \Delta_{\eta_{22}}]_j d\tau \\ & - \int_{T_0}^{T_d} e^{-\alpha(t-\tau)} [\Delta_{\xi(\cdot)}]_j d\tau \end{aligned} \tag{37}$$

and (37) still holds for $t > T_d$. From the incipient fault detection decision, a necessary requirement to detect the incipient fault at T_d is that there is a j, $j = 1, \cdots, 2q$ such that $\Delta_{rj}(t) < 0$ for $t \geq T_d$, that is

$$\begin{aligned} & \int_{T_0}^{T_d} e^{-\alpha(t-\tau)} [\Delta_{\xi(\cdot)}]_j d\tau \\ & \geq \Delta_{rj}(T_0) + \int_{T_0}^{T_d} e^{-\alpha(t-\tau)} [D_\Delta(v - e_1) + \Delta_{\eta_{22}}]_j d\tau \end{aligned} \tag{38}$$

and (38) still holds for $t > T_d$.

Remark 8: Inequality (38) provides a method to judge whether an incipient sensor fault can be detected. For example, if $\Delta_{rj}(T_0) = 0$ and $0 \leq [D_\Delta(v - e_1) + \Delta_{\eta_{22}}]_j \leq \delta(t)$ where $\delta(t)$ is a positive function, then the faults with their magnitudes $[\Delta_{\xi(\cdot)}]_j$ satisfying $[\Delta_{\xi(\cdot)}]_j \geq \delta(t)$ for $t > T_0$ can be detected. More specifically, $\delta(t)$ can be chosen as $\delta(t) = \delta_0 + e^{-\beta t}$ with $\delta_0 > 0$ and $\beta > 0$ in the transition process. So the detectability of the developed incipient sensor fault detection scheme will increases as T_0 increases. ∇

Remark 9: The left hand side of (38) can be seen as the first-order filter with single pole $-\alpha$ which can increase the response rates of r and J_{th} and reduce the incipient fault detection time T_d by increasing the value of α. Hence, the value of α should be chosen large sufficient to detect the incipient faults in a short time. In addition, to increase the incipient fault detectability, it can be seen from the right hand side of (38) that the l_1-norm of vector $D_\Delta(v - e_1)$ should be reduced by adjusting nonnegative matrices F_1 and F_2. Recalling the dynamics of e_1 and v in (13) and (14) respectively, the negative effect of $D_\Delta(v - e_1)$ can be reduced by solving the linear programming problem on the variables F_1 and F_2 presented by Theorem 3.4 in [32]. ∇

Remark 10: Comparing with the adaptive thresholds presented in [7] and [33], the adaptive threshold J_{th} in this paper is generated by (34) without using absolute value, which facilitates to give a fair judgment for ISFD in all directions and improve fault detectability. The reason can be seen from the sufficient condition (38) which is more relax than the similar condition in [7] and [33] using absolute value. ∇

Remark 11: This paper uses the interval estimation technique to design diagnostic observer for a class of nonlinear control systems, which is quite challenging because there is no existing proper interval models for the nonlinearities $g_1(x_1, y, u)$, $g_{21}(x_1, y, u)$ and $g_{22}(x_1, y, u)$ considered in (6)-(8). This paper introduces the proper interval model $[\underline{\varphi}_1, \bar{\varphi}_1]$ for $g_1(x_1, y, u)$ in (A.2) and similar interval model for $g_{22}(x_1, y, u)$ satisfying (32)-(33) based on Lemma 2. Then these optimized interval models are used to develop dynamical interval estimator (10)-(11) where the Hurwitz and Metzler matrix $\bar{A}_{11}$ is introduced to guarantee the stability of the time-varying system (13), and is also used to develop residual generator (31) and threshold generator (34). Furthermore, based on Lemma 2, the inequality (23) is yielded, which facilitates to design gains $m_1(\cdot)$ and $M_2(\cdot)$ in (26) and (27) respectively and guarantees that the sliding mode with respect to the sliding surface $\mathscr{L}$ occurs and maintains on it thereafter. Therefore, one contribution of this paper is developing an ISMO as diagnostic observer for a class of continuous nonlinear systems.

On the other hand, because of the novel interval models for the considered nonlinearities, the ISFD schemes proposed in this paper, including residual generator (31), threshold generator (34) and the incipient fault detectability, are further developed, and a set of sufficient detectable conditions (38) is proposed. Therefore, another contribution of this paper is that an ISFD is established with new residual generator and threshold generator. ∇

V. Verifications

This section will give two verification examples, including a numerical example and an application example to show the universality of the proposed incipient sensor fault detection method. Also, comparisons with existing sensor fault detection method such as presented in [7] and [33] are presented to illustrate advantages of the proposed method.

A. Numerical Example

Consider a simple nonlinear system in the form of (6)-(9) as follows:

$$\begin{aligned}\dot{x}_1 =& -80x_1 + 5x_2 + x_1^2 + \eta_1,\\ \dot{x}_2 =& -x_1 - 5x_2 + \eta_{21},\\ \dot{x}_3 =& x_1 - 10x_3 + x_1^2 + \xi + \eta_{22}\end{aligned}$$

where $\eta_1 = 10(\sin(20t) + \sin(25t))$, $\eta_{21} = 10(1.2 + \sin(20t) + \sin(35t))$ and $\eta_{22} = -5(\sin(18t) + \sin(20t))$. The item ξ is the fault-related signal, which is set as $\xi = 0$ for $t < 0.5s$ and $\xi = 10 + 5\sin(250t)$ for $t \geq 0.5s$. The term x_1^2 is the continuous nonlinearity whose new interval model will be designed based on the method presented in *Appendix A*.

Firstly, $\underline{\eta}_1$, $\bar{\eta}_1$, $\bar{\eta}_{21}$, $\underline{\eta}_{22}$ and $\bar{\eta}_{22}$ in Assumption 1 are selected as $\bar{\eta}_1 = 10(0.1 + \sin(20t) + \sin(25t))$, $\underline{\eta}_1 = 10(-0.2 + \sin(20t) + \sin(25t))$, $\bar{\eta}_{21} = |10(2 + \sin(20t) + \sin(35t))|$, $\bar{\eta}_{22} = -5(-0.5 + \sin(18t) + \sin(20t))$, $\underline{\eta}_{22} = -5(0.3 + \sin(18t) + \sin(20t))$, respectively. Then, based on *Appendix A*, for $x_1 \in [-5, 5]$,

$$\begin{aligned}\underline{\mathbb{A}}_1(\bar{x}_1, \cdot) = 0,\ \underline{\mathbb{W}}_1(\bar{x}_1, \cdot) = -2\bar{x}_1,\\ \bar{\mathbb{A}}_1(\underline{x}_1, \cdot) = -\underline{x}_1^2 + 0.25(\underline{x}_1 + 5),\ \bar{\mathbb{W}}_1(\underline{x}_1, \cdot) = -0.25,\\ \underline{\mathbb{A}}_{22}(\bar{x}_1, \cdot) = 0,\ \underline{\mathbb{W}}_{22}(\bar{x}_1, \cdot) = -2\bar{x}_1,\\ \bar{\mathbb{A}}_{22}(\underline{x}_1, \cdot) = -\underline{x}_1^2 + 0.25(\underline{x}_1 + 5), \bar{\mathbb{W}}_{22}(\underline{x}_1, \cdot) = -0.25.\end{aligned}$$

Based on Propositions 1 and 2, the design parameters $F_1 = 15$ and $\kappa = 10$. The parameter F_2 in (29) and (30) is chosen as 0. Thus, the interval sliding mode diagnostic observer (10)-(11) and (20) can be constructed and residuals and adaptive threshold can also be generated by (31) and (34) respectively. Their time responses are shown in Figs. 1-2. It can be seen from Fig. 1 that $\bar{x}_1 \leq x_1 \leq \underline{x}_1$ for $t > 0$, and the estimate error e_2 is driven to the sliding surface in finite time and maintains on it thereafter. Fig. 2 shows that for $t > 0.5s$, r_1 exceeds J_{th1} and maintains larger than J_{th1}, and the variable Γ_1 becomes 1 at T_d and maintains unchanged. Therefore, based on the ISFD decision principle, the incipient sensor fault is detected at time instant T_d.

The adaptive threshold concept proposed in [7] and [33] motivates this paper to use interval estimation techniques to design adaptive thresholds for incipient sensor fault detection schemes. In addition, [7] and [33] are quite popular in fault diagnosis areas with high citations. Therefore, in this simulation, the comparison will be made between the developed fault diagnosis method in this paper and the results in [7] and [33].

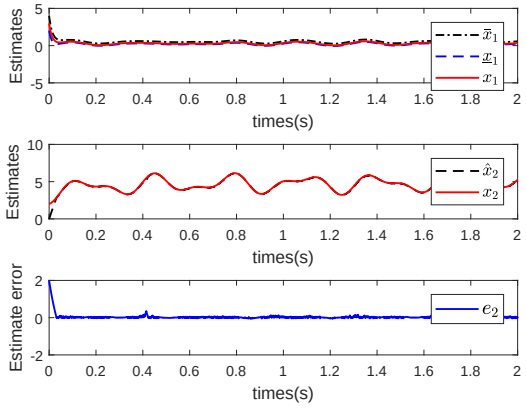

Fig. 1. Time responses of $\bar{x}_1$, x_1, $\underline{x}_1$, $\hat{x}_2$, x_2 and e_2.

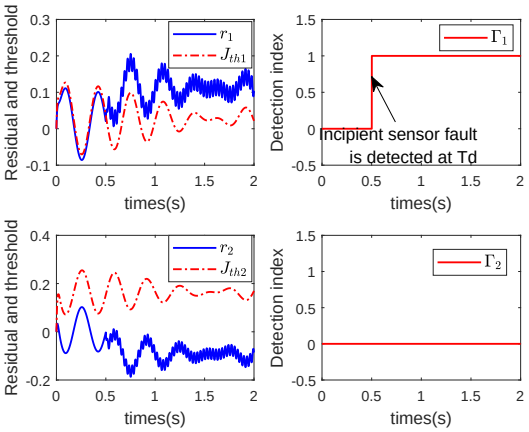

Fig. 2. Time responses of r, J_{th}, Γ_1 and Γ_2.

It should be pointed out that this paper has different design parameters compared with [7] and [33]. But to make this comparison persuasive, their design parameters with similar functions are chosen as the same. To design residual generator, that is the dynamic of $\hat{x}_3$, the gain matrix in [7] and [33] is chosen as F_2. Similar with the selection before, the estimate error $x_3 - \hat{x}_3$ is chosen as r because ξ appears only in x_3. In addition, the bound of η_{22} is also chosen as $\max\{|\bar{\eta}_{22}|, |\underline{\eta}_{22}|\} = 5(0.5 + |\sin(18t)| + |\sin(20t)|)$.

The estimates and fault detection results are presented in Figs. 3 and 4. Fig. 3 illustrates the estimates for x_1 and x_2. By comparing Fig. 1 with Fig. 3, it can be seen that Fig. 1 provides better estimates than Fig. 3. Comparing the time responses of r and J_{th} in Fig. 4 with ones in Fig. 2, it is easy to see that the adaptive thresholds in Fig. 2 are closer to the residuals than that in Fig. 4 for $t < 0.5s$ (in fault-free scenario), which means that the adaptive thresholds in Fig. 2 are more proper than that

in Fig. 4. The different time responses of Γ in Fig. 4 and Fig. 2 also show the advantage of the ISFD method proposed in this paper. The variable Γ_1 in Fig. 2 becomes 1 at T_d and maintains it for $t > T_d$. However, the variable Γ in Fig. 4 varies between 1 and 0 intermittently and can not maintain value 0. Therefore, based on the developed fault detection decision principle, the same incipient sensor fault is detected based on Fig. 2 while is not detected based on Fig. 4.

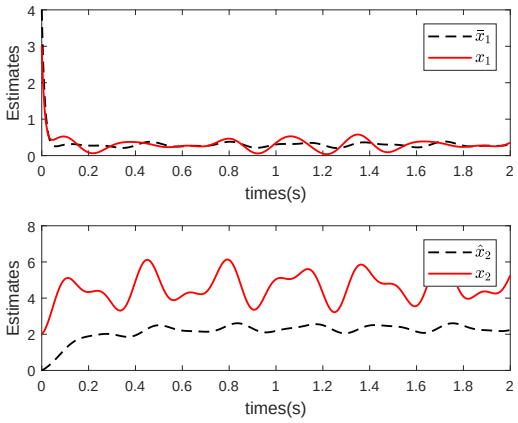

Fig. 3. Time responses of $\hat{x}_1$, $\hat{x}_2$, x_1 and x_2.

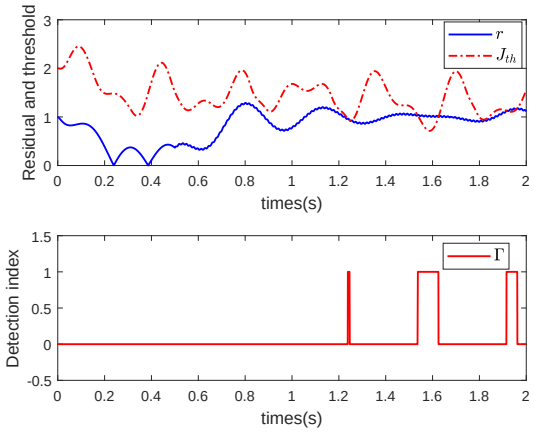

Fig. 4. Time responses of r, J_{th} and Γ.

B. Application Example

To verify the theoretical results developed in this paper using traction devices in CRH, faults should be injected firstly. The hardware-implemented and simulation-implemented fault injection are two main fault injection techniques [35]. The latter has some advantages such as high observability, controllability and short test period, and has become the mainstream in fault injection areas [36]. In this section, the developed ISFD method will be applied to a simulation and verification platform, called traction and driving control system-fault injection benchmark (TDCS-FIB). This platform was developed using a simulation-implemented fault injection by a professional team (Central South University Fault Injection Team) and was built on SimPower System toolbox. This platform is able to simulate faults in traction converters, traction motors, sensors and traction control units for CRH effectively [36]. The structure of this platform is shown in Fig. 5 outside of the red rectangle frame, which consists of fault injection modules and the traction and driving control system.

The red rectangle frame in Fig. 5 is fault diagnosis schemes. The circuit topology of the rectifier device is shown in Fig. 6

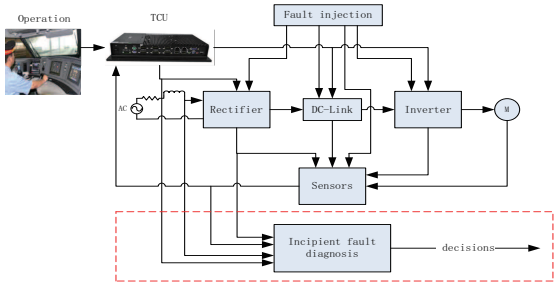

Fig. 5. Schematic diagram of TDCS-FIB.

where u_s and i_s are the voltage and current of the grid side, R and L are the resistance and inductance of the grid side respectively, S_{ia}, S_{ib}, $i = 1, 2, 3, 4$ are the IGBT modules of a and b bridges, respectively, u_1 and u_2 are dc voltages in dc-link side respectively, and i_L is the load current. Parameters are given by Table I. Suppose that there is no power loss and

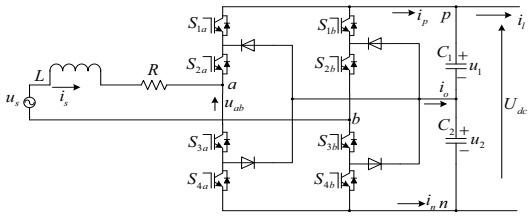

Fig. 6. Single-phase three-level diode clamp PWM rectifier.

TABLE I
PARAMETERS.

Parameter	Value	Unit
P_m	800	KW
R	0.34	Ω
L	2.2×10^{-3}	H
C_1	16×10^{-3}	F
C_2	16×10^{-3}	F
u_s	$2100 \sin(314t)$	V

energy storage in the traction motors and inverters. Then

$$(u_1 + u_2)i_l = P_m$$

where P_m is the instantaneous power of the traction motors. It is supposed that P_m is fixed.

The harmonics in i_s, u_1 and u_2 are considered as disturbances and uncertainties and denoted by $\eta_n(u_s, i_s, u_1, u_2, \omega, t) = [\eta_{i_s}(\cdot), \eta_{u_1}(\cdot), \eta_{u_2}(\cdot)]^\top$. Then, based on method provided in [37]

and the average modeling approach presented in [38] , the dynamic model of this rectifier is obtained by

$$\begin{aligned}\frac{di_s}{dt} =&\frac{1}{L}\left(u_s - Ri_s - u_{ab}\right) + \eta_{i_s}(\cdot),\\ \frac{du_1}{dt} =&\frac{1}{C_1}\left(i_p - i_l\right) - \beta u_1 - \frac{P_m}{u_1+u_2} + \eta_{u_1}(\cdot),\\ \frac{du_2}{dt} =&\frac{1}{C_2}\left(-i_n - i_l\right) - \beta u_2 - \frac{P_m}{u_1+u_2} + \eta_{u_2}(\cdot)\end{aligned}$$

where β is a positive constant and obtained using the average modeling approach, which is chosen as $\beta = 100$ in this simulation. In this simulation, incipient sensor fault detection schemes are aimed to supervise the voltage sensors. These two potential incipient voltage sensor faults are modeled as (3) where A_f is given as follows

$$A_f = \begin{bmatrix} -0.5 & 0 \\ 2 & -0.5 \end{bmatrix}.$$

Let $z := \mathrm{col}(Z, f)$. Then the dynamic model which has the form of (4)-(5) can be obtained, and there exists a coordinate transformation $x = Tz$ where

$$T = \begin{bmatrix} 0 & -1.4142 & 0 & 0 & 0 \\ 0 & 0 & 1.4142 & 0 & 0 \\ 1 & 0 & 0 & 0 & 0 \\ 0 & 0 & -1 & 0 & -1 \\ 0 & -1 & 0 & -1 & 0 \end{bmatrix}$$

such that the augmented system has the form (6)-(9) in new coordinates. Moreover, in the new coordinates, $i_s = x_3$, $u_1 = -0.707x_1$ and $u_2 = -0.707x_2$. Then

$$g_1(x) = \begin{bmatrix} -\frac{1\times10^7}{x_1+x_2} \\ -\frac{1\times10^7}{x_1+x_2} \end{bmatrix},\ g_{21}(x) = 0,\ g_{22}(x) = \begin{bmatrix} -\frac{2.8284\times10^6}{x_1+x_2} \\ -\frac{2.8284\times10^6}{x_1+x_2} \end{bmatrix}.$$

The dc link voltages u_1 and u_2 locate between 1000V and 2000V in traction systems. Then a hypercube set Ω with 4 vertices is obtained where $u_{\min} = [-1414, -1414]^\top$ and $u_{\max} = [-2828, -2828]^\top$. Then the coordinates of these four vertices are given by $[-1414, -1414]$, $[-1414, -2828]$, $[-2828, -1414]$ and $[-2828, -2828]$. In order to construct the closed form solution for the min-max optimization problem in (2) for $g_1(x)$, $g_{21}(x)$ and $g_{22}(x)$, a 2-dimensional simplex Ω_s, enclosing Ω is constructed. The vertices of Ω_s are given by $[0, -1414]$, $[-2828, -1414]$ and $[-2828, -4242]$. Then the solutions based on the method provided in [24] are presented as follows

$$\begin{aligned}[\bar{a}_{11}(\bar{x}_1), \bar{w}_{11}(\bar{x}_1)]^T =& \begin{bmatrix} -1 & -\bar{x}_1 & -\bar{x}_2-1414 \\ -1 & -\bar{x}_1-2828 & -\bar{x}_2-1414 \\ -1 & -\bar{x}_1-2828 & -\bar{x}_2-4242 \end{bmatrix}^{-1} \begin{bmatrix} -\frac{1\times10^7}{\bar{x}_1+\bar{x}_2}-7072.1 \\ -\frac{1\times10^7}{\bar{x}_1+\bar{x}_2}-2357.4 \\ -\frac{1\times10^7}{\bar{x}_1+\bar{x}_2}-1414.4 \end{bmatrix},\\ [\bar{a}_{12}(\bar{x}_1), \bar{w}_{12}(\bar{x}_1)] =& [\bar{a}_{11}(\bar{x}_1), \bar{w}_{11}(\bar{x}_1)],\\ [\underline{a}_{11}(\underline{x}_1), \underline{w}_{11}(\underline{x}_1)] =& [0, -\tfrac{1\times10^7}{(\underline{x}_1+\underline{x}_2)^2}, -\tfrac{1\times10^7}{(\underline{x}_1+\underline{x}_2)^2}],\\ [\underline{a}_{12}(\underline{x}_1), \underline{w}_{12}(\underline{x}_1)] =& [\underline{a}_{11}(\underline{x}_1), \underline{w}_{11}(\underline{x}_1)],\\ \mathbb{W}_{21}(\cdot) =& 0,\ \mathbb{A}_{21}(\cdot) = 0,\\ [\underline{a}_{221}(\bar{x}_1),\ \underline{w}_{221}(\bar{x}_1)] =& [0, -\tfrac{2.8284\times10^6}{(\bar{x}_1+\bar{x}_2)^2}, -\tfrac{2.8284\times10^6}{(\bar{x}_1+\bar{x}_2)^2}],\\ [\underline{a}_{222}(\bar{x}_1),\ \underline{w}_{222}(\bar{x}_1)] =& [\underline{a}_{221}(\bar{x}_1),\ \underline{w}_{221}(\bar{x}_1)],\\ \left[\bar{a}_{221}(\underline{x}_1), \bar{w}_{221}(\underline{x}_1)\right]^T =& \begin{bmatrix} -1 & -\underline{x}_1 & -\underline{x}_2-1414 \\ -1 & -\underline{x}_1-2828 & -\underline{x}_2-1414 \\ -1 & -\underline{x}_1-2828 & -\underline{x}_2-4242 \end{bmatrix}^{-1} \begin{bmatrix} -\frac{2.8284\times10^6}{\underline{x}_1+\underline{x}_2}-5000.8 \\ -\frac{2.8284\times10^6}{\underline{x}_1+\underline{x}_2}-1666.9 \\ -\frac{2.8284\times10^6}{\underline{x}_1+\underline{x}_2}-1000.2 \end{bmatrix},\\ \left[\bar{a}_{222}(\underline{x}_1), \bar{w}_{222}(\underline{x}_1)\right] =& \left[\bar{a}_{221}(\underline{x}_1), \bar{w}_{221}(\underline{x}_1)\right].\end{aligned}$$

Thus, nonlinear functions $\underline{\varphi}_1\left(\bar{x}_1, \underline{x}_1, \cdot\right)$ and $\bar{\varphi}_1\left(\bar{x}_1, \underline{x}_1, \cdot\right)$ in (A.2), and $(\underline{\mathbb{A}}_1 + \bar{\mathbb{A}}_1)(\bar{x}_1, \cdot)$, $\left(\underline{\mathbb{W}}_1^- + \bar{\mathbb{W}}_1^+\right)(\bar{x}_1, \cdot)$, $\bar{\mathbb{W}}_1^+(\bar{x}_1, \cdot)$ $(\underline{\mathbb{A}}_1 + \bar{\mathbb{A}}_1)(\underline{x}_1, \cdot)$, $(\bar{\mathbb{W}}_1^- + \bar{\mathbb{W}}_1^+)(\underline{x}_1, \cdot)$, $\bar{\mathbb{W}}_1^+(\underline{x}_1, \cdot)$ in (A.5) and (A.6) are obtained, respectively. Also, $-\underline{\mathbb{W}}_{22}^-(\bar{x}_1, \cdot)\bar{w} + \underline{\mathbb{A}}_{22}(\bar{x}_1, \cdot)$,$-\bar{\mathbb{W}}_{22}^-(\underline{x}_1, \cdot)\underline{w} + \bar{\mathbb{A}}_{22}(\underline{x}_1, \cdot)$ in (34) are obtained. Then, based on Proposition 1, the gain matrix F_1 is calculated using LMI technique and shown as follows

$$F_1 = \begin{bmatrix} 38.1067 & 6.4006 \\ 6.4006 & 38.1067 \end{bmatrix}.$$

In the sub-observer (20), the gain matrix $\hat{A}_{22}^{21} = -100$. The gains m_{21} and M_{21} are chosen based on Proposition 2. Then the residual generator (31) and threshold generator (34) are constructed with $\hat{A}_{22}^{22} = -100I_2$ and

$$F_2 = \begin{bmatrix} 1.4142 & 70.3571 \\ 70.3571 & 0 \end{bmatrix}. \tag{39}$$

In the disturbance η_{i_s}, the 3rd-order and the 5th-order harmonics of grid side current i_s are mainly considered because their amplitudes are larger than other higher order harmonics. Also, parameter uncertainties $\Delta_R = 0.02\Omega$, $\Delta_L = 0.2 \times 10^{-4}$H and $\Delta_C = 2 \times 10^{-4}$F are considered. Then,

$$\begin{aligned}\eta_{i_s} =& \frac{H_3 i_s}{\sqrt{2}\cos(\omega t)}\sin(3\omega t) + \frac{H_5 i_s}{\sqrt{2}}\sin(5\omega t - \varphi_5) + \Delta_{1i_s} i_s,\\ \eta_{u_1} =& \Delta_{1u_1} i_s,\ \eta_{u_2} = \Delta_{1u_2} i_s\end{aligned}$$

where $H_3 = 100$, $H_5 = 20$ and phase angle $\varphi_5 = 0.1\pi$, $\Delta_{1u_1} = -0.7716$ and $\Delta_{1u_2} = 0.7716$. Thus,

$$\begin{aligned}\eta_1 =& -1.414[\Delta_{1u_1} y_1, \Delta_{1u_2} y_1]^T,\\ \eta_{21} =& \frac{\sqrt{2}H_3 y_1}{\cos(\omega t)}\sin(3\omega t) + \sqrt{2}H_5 y_1 \sin(5\omega t - \varphi_5) + \Delta_{1i_s} y_1,\\ \eta_{22} =& -[\Delta_{1u_2} y_1, \Delta_{1u_1} y_1]^T.\end{aligned}$$

Therefore, $\bar{\eta}_{21}(\cdot)$, $\underline{\eta}_1(\cdot)$, $\bar{\eta}_1(\cdot)$, $\underline{\eta}_{22}(\cdot)$ and $\bar{\eta}_{22}(\cdot)$ in Assumption 1 are selected as

$$\bar{\eta}_1(\cdot) = [|1.414\Delta_{u_1} y_1|,\ |1.414\Delta_{u_2} y_1|]^\top,$$
$$\underline{\eta}_1(\cdot) = [-|1.414\Delta_{u_1} y_1|,\ -|1.414\Delta_{u_2} y_1|]^\top,$$
$$\bar{\eta}_{21}(\cdot) = \left\| \frac{\sqrt{2}H_3 y_1}{\cos(\omega t)} \sin(3\omega t) + \sqrt{2}H_5 y_1 \sin(5\omega t - \varphi_5) + \Delta_{1i_s} y_1 \right\|,$$
$$\bar{\eta}_{22}(\cdot) = [|\Delta_{u_2} y_1|,\ |\Delta_{u_1} y_1|]^T,\ \underline{\eta}_{22}(\cdot) = [-|\Delta_{u_2} y_1|,\ -|\Delta_{u_1} y_1|]^\top.$$

In addition, the vector $\xi(t)$ in (3) to describe the incipient voltage sensor faults is given by $\xi(t) = \mathrm{col}(\xi_1, \xi_2)$ where

$$\xi_1 = \begin{cases} 0, & t \le 0.5s, \\ 100 + 20\sin(200t), & t \ge 0.5s, \end{cases}$$
$$\xi_2 = \begin{cases} 0, & t \le 0.5s, \\ 100 + 50\sin(200t), & t \ge 0.5s. \end{cases}$$

The simulation results are shown in Figs. 7-11. It can be seen from Figs. 7 and 8 that the designed interval observer (10)-(11) can guarantee that $\underline{x}_1 < x_1 < \bar{x}_1$ for $t \ge 0$. Fig. 9 illustrates the estimate $\hat{x}_{21}$ and estimate error e_{21}, which shows that the sliding mode takes place in finite time and maintains on sliding surface for $t \ge 0.002s$. From Fig. 10, it is obtained that residuals r (blue and solid lines) are lower than the corresponding adaptive thresholds J_{th} (red and dashed lines) for $t < T_0$ ($T_0 = 0.5s$), while r_3 exceeds J_{th3} intermittently and r_4 exceeds J_{th4} for $t > T_0$. Fig. 11 illustrates the fault decision index Γ, and it can be seen from this figure that the incipient dc voltage sensor faults are detected at time T_d.

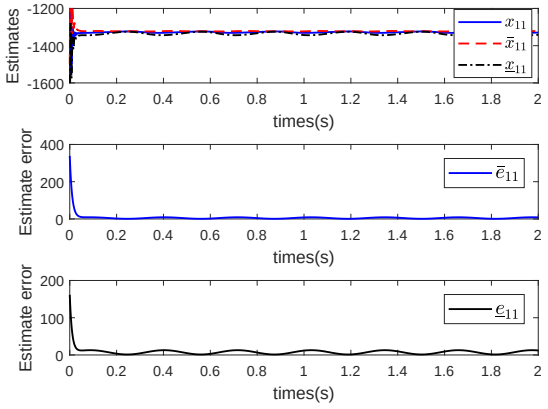

Fig. 7. Time responses of $\bar{x}_{11}$, x_{11}, $\underline{x}_{11}$, $\bar{e}_{11}$ and $\underline{e}_{11}$.

To compare with existing sensor fault detection methods, the method proposed in [7] and [33] is constructed for this application example and the fault detection results are presented in Fig. 13 where the estimate errors $x_4 - \hat{x}_4$ and $x_5 - \hat{x}_5$ are chosen as r_1 and r_2 respectively. In addition, the norm bounds of elements in η_{22}, i.e. $|\Delta_{u_2} y_1|$ and $|\Delta_{u_1} y_1|$, are selected to generate adaptive thresholds presented in [7] and [33]. By comparing the time responses of r and J_{th} in Fig. 13 with Fig. 10, the similar conclusion with that in *Numerical Example* is obtained, that is the adaptive thresholds in Fig. 10 are more proper than that in Fig. 13. On the other hand, it is shown in

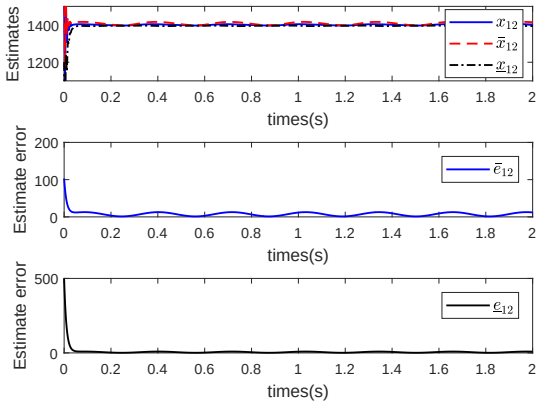

Fig. 8. Time responses of $\bar{x}_{12}$, x_{12}, $\underline{x}_{12}$, $\bar{e}_{12}$ and $\underline{e}_{12}$.

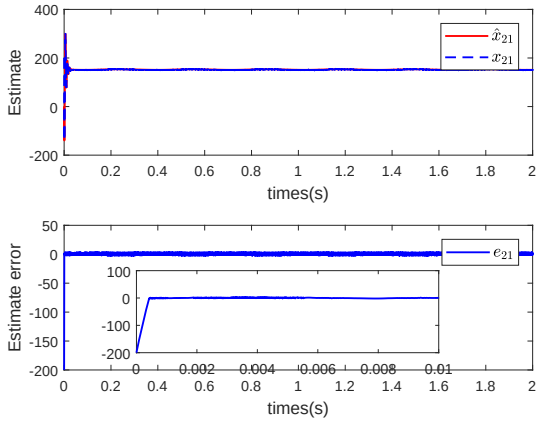

Fig. 9. Time responses of $\hat{x}_{21}$ and e_{21}.

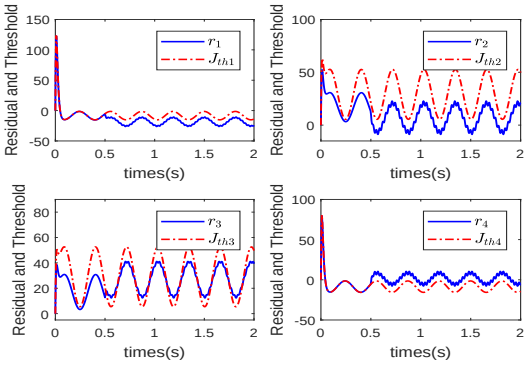

Fig. 10. Time responses of residual r and threshold J_{th}.

Fig. 11 that the variable Γ_4 becomes 1 at T_d and maintains on it for $t > T_d$, while both the variables Γ_1 and Γ_2 in Fig. 13 maintain 0 for $t > 0$. Therefore, based on the developed fault detection decision principle, the same incipient sensor fault is detected based on Fig. 11. However, this fault can not be detected based on Fig. 13.

Therefore, compared with [7] and [33], superiorities of the developed incipient sensor fault detection method are

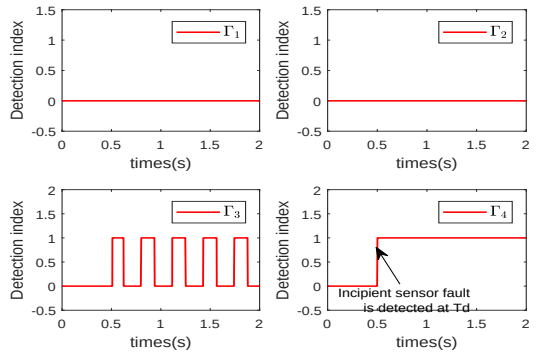

Fig. 11. Time responses of Γ_i, $i = 1, 2, 3, 4$.

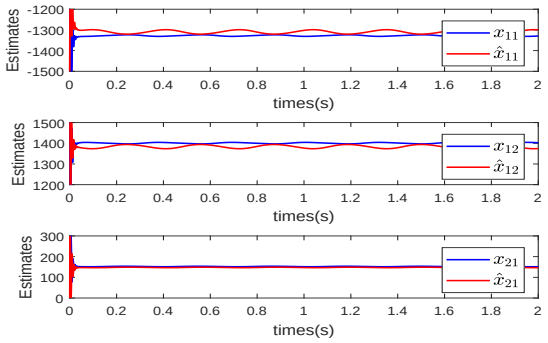

Fig. 12. Time responses of $\hat{x}_{11}$, $\hat{x}_{12}$, $\hat{x}_{21}$, x_{11}, x_{12} and x_{21}.

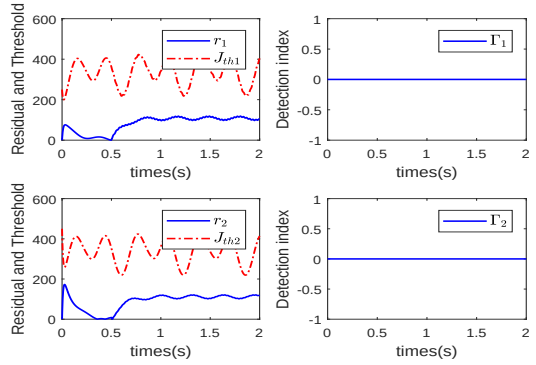

Fig. 13. Time responses of residual r, threshold J_{th}, Γ_1 and Γ_2.

summarized as follows:

- The proposed interval sliding mode observer provides better estimates than the diagnostic observer used in [7] and [33] because interval estimation techniques and sliding mode techniques are applied together.
- The developed incipient sensor fault detection method has higher fault detectability than the ones developed in [7] and [33] because the better estimates are provided by the proposed novel ISMO and double independent adaptive thresholds are developed using more precise interval bounds of uncertainties.

VI. Conclusions

This paper has proposed a new ISFD method based on an ISMO for a class of nonlinear systems with observer unmatched uncertainties. An interval estimator and sliding mode estimator have been designed. Then residual generator and adaptive threshold generator have been proposed. Incipient sensor fault detection decision scheme and fault detectability have also been studied. At last, an application for detecting incipient dc voltage sensor faults of rectifiers is presented to demonstrate the effectiveness and practicality of the proposed incipient faults detection schemes. Fault diagnosis for systems with uncertain structural parameters using interval estimation technique is a challenging problem, which will be addressed in the future work. On the other hand, the incipient fault description method in this paper can only characterize the continuous property but not small amplitude property of incipient faults. This leads to that the incipient sensor fault detection scheme developed in this paper is not able to optimize the design parameters to specially improve the incipient fault detectability. In the future work, novel description methods for incipient faults should be developed to characterize both the continuous and small amplitude properties.

Appendix A

Let $\bar{x}_1$ and $\underline{x}_1$ be estimates of the upper bound and lower bound of x_1 respectively and suppose that $\bar{x}_1$, $\underline{x}_1 \in \Omega$. Then based on Lemma 2, for $g_{1i}(x_1, \cdot)$ in $x_1 \in \Omega$, the ith element of $g_1(x_1, \cdot)$, and $\bar{x}_1$, $\underline{x}_1 \in \Omega$, there exist a scalar $a_{1i}(\cdot)$ and a vector $w_{1i}(\cdot)$ such that (1) holds. Denote that

$$\begin{cases} w_{1i}(\cdot) = \bar{w}_{1i}(\cdot), \ a_{1i}(\cdot) = \bar{a}_{1i}(\cdot), \ \alpha > 0, \\ w_{1i}(\cdot) = \underline{w}_{1i}(\cdot), \ a_{1i}(\cdot) = \underline{a}_{1i}(\cdot), \ \alpha < 0. \end{cases}$$

It follows from Lemma 2 that

$$\begin{aligned} g_{1i}(x_1, \cdot) \leq & g_{1i}(\bar{x}_1, \cdot) + \bar{w}_{1i}(\bar{x}_1, \cdot)\bar{x}_1 - \bar{w}_{1i}(\bar{x}_1, \cdot)x_1 + \bar{a}_{1i}(\bar{x}_1, \cdot), \\ g_{1i}(x_1, \cdot) \geq & g_{1i}(\underline{x}_1, \cdot) + \underline{w}_{1i}(\underline{x}_1, \cdot)\underline{x}_1 - \underline{w}_{1i}(\underline{x}_1, \cdot)x_1 - \underline{a}_{1i}(\underline{x}_1, \cdot). \end{aligned}$$

For $\underline{x}_1 \leq x_1 \leq \bar{x}_1$, it follows from Lemma 1 that

$$\begin{aligned} \bar{w}_{1i}^+(\cdot)\underline{x}_1 - \bar{w}_{1i}^-(\cdot)\bar{x}_1 \leq \bar{w}_{1i}(\bar{x}_1, \cdot)x_1 \leq \bar{w}_{1i}^+(\cdot)\bar{x}_1 - \bar{w}_{1i}^-(\cdot)\underline{x}_1, \\ \underline{w}_{1i}^+(\cdot)\underline{x}_1 - \underline{w}_{1i}^-(\cdot)\bar{x}_1 \leq \underline{w}_{1i}(\underline{x}_1, \cdot)x_1 \leq \underline{w}_{1i}^+(\cdot)\bar{x}_1 - \underline{w}_{1i}^-(\cdot)\underline{x}_1. \end{aligned}$$

Thus,

$$\underline{\varphi}_{1i}\left(\bar{x}_1, \underline{x}_1, \cdot\right) \leq g_{1i}(x_1, \cdot) \leq \bar{\varphi}_{1i}\left(\bar{x}_1, \underline{x}_1, \cdot\right) \tag{A.1}$$

where

$$\begin{aligned} \bar{\varphi}_{1i}\left(\bar{x}_1, \underline{x}_1, \cdot\right) = & g_{1i}(\bar{x}_1, \cdot) + \bar{w}_{1i}(\bar{x}_1, \cdot)\bar{x}_1 + \bar{w}_{1i}^-(\bar{x}_1, \cdot)\bar{x}_1 \\ & - \bar{w}_{1i}^+(\bar{x}_1, \cdot)\underline{x}_1 + \bar{a}_{1i}(\bar{x}_1, \cdot), \\ \underline{\varphi}_{1i}\left(\bar{x}_1, \underline{x}_1, \cdot\right) = & g_{1i}\left(\underline{x}_1, \cdot\right) + \underline{w}_{1i}\left(\underline{x}_1, \cdot\right)\underline{x}_1 + \underline{w}_{1i}^-\left(\underline{x}_1, \cdot\right)\underline{x}_1 \\ & - \underline{w}_{1i}^+\left(\underline{x}_1, \cdot\right)\bar{x}_1 - \underline{a}_{1i}\left(\underline{x}_1, \cdot\right). \end{aligned}$$

Moreover, let $\bar{e}_1 = \bar{x}_1 - x_1$ and $\underline{e}_1 = x_1 - \underline{x}_1$, it follows from Lemma 2 that

$$\begin{aligned} g_{1i}(\bar{x}_1, \cdot) - g_{1i}(x_1, \cdot) \leq & \underline{a}_{1i}(\bar{x}_1, \cdot) - \underline{w}_{1i}(\bar{x}_1, \cdot)\bar{e}_1, \\ g_{1i}(x_1, \cdot) - g_{1i}(\underline{x}_1, \cdot) \leq & \bar{a}_{1i}(\underline{x}_1, \cdot) - \bar{w}_{1i}(\underline{x}_1, \cdot)\underline{e}_1. \end{aligned}$$

Therefore, there exist vectors $\bar{\mathbb{A}}_1 = [\bar{a}_{1i}]^\top$, $\underline{\mathbb{A}}_1 = [\underline{a}_{1i}]^\top$, $\bar{\varphi}_1 = [\bar{\varphi}_{1i}]^\top$ and $\underline{\varphi}_1 = [\underline{\varphi}_{1i}]^\top$, and diagonal matrix $\bar{\mathbb{W}}_1 = \text{diag}\{\bar{w}_{1i}\}$, $\underline{\mathbb{W}}_1(\cdot) = \text{diag}\{\underline{w}_{1i}\}$ such that for $\underline{x}_1 < x_1 < \bar{x}_1$,

$$g_1(x_1,\cdot) \in \left[\underline{\varphi}_1\left(\bar{x}_1,\underline{x}_1,\cdot\right), \bar{\varphi}_1\left(\bar{x}_1,\underline{x}_1,\cdot\right)\right], \tag{A.2}$$

$$g_1(\bar{x}_1,\cdot) - g_1(x_1,\cdot) \le \underline{\mathbb{A}}_1(\bar{x}_1,\cdot) - \underline{\mathbb{W}}_1(\bar{x}_1,\cdot)\bar{e}_1, \tag{A.3}$$

$$g_1(x_1,\cdot) - g_1\left(\underline{x}_1,\cdot\right) \le \bar{\mathbb{A}}_1(\underline{x}_1,\cdot) - \bar{\mathbb{W}}_1(\underline{x}_1,\cdot)\underline{e}_1. \tag{A.4}$$

Moreover,

$$\begin{aligned} 0 \le \bar{\varphi}_1\left(\bar{x}_1,\underline{x}_1,\cdot\right) - g_1(x_1,\cdot) \le{}& (\underline{\mathbb{A}}_1 + \bar{\mathbb{A}}_1)(\bar{x}_1,\cdot) \\ & - \underline{\mathbb{W}}_1(\bar{x}_1,\cdot)\bar{e}_1 + \bar{\mathbb{W}}_1^+(\bar{x}_1,\cdot)\left(\bar{e}_1 + \underline{e}_1\right), \\ 0 \le g_1(x_1,\cdot) - \underline{\varphi}_1\left(\bar{x}_1,\underline{x}_1,\cdot\right) \le{}& (\underline{\mathbb{A}}_1 + \bar{\mathbb{A}}_1)(\underline{x}_1,\cdot) \\ & - \bar{\mathbb{W}}_1(\underline{x}_1,\cdot)\underline{e}_1 + \underline{\mathbb{W}}_1^+(\underline{x}_1,\cdot)\left(\bar{e}_1 + \underline{e}_1\right). \end{aligned}$$

Since $\underline{\mathbb{W}}_1^+(\cdot) \ge 0$, $\bar{\mathbb{W}}_1^+(\cdot) \ge 0$, $-\underline{\mathbb{W}}_1(\cdot)\bar{e}_1 \le \underline{\mathbb{W}}_1^-(\cdot)\bar{e}_1$ and $-\bar{\mathbb{W}}_1(\cdot)\underline{e}_1 \le \bar{\mathbb{W}}_1^-(\cdot)\underline{e}_1$,

$$\begin{aligned} 0 \le \bar{\varphi}_1\left(\bar{x}_1,\underline{x}_1,\cdot\right) - g_1(x_1,\cdot) \le{}& (\underline{\mathbb{A}}_1 + \bar{\mathbb{A}}_1)(\bar{x}_1,\cdot) \\ & + \left(\underline{\mathbb{W}}_1^- + \bar{\mathbb{W}}_1^+\right)(\bar{x}_1,\cdot)\bar{e}_1 + \bar{\mathbb{W}}_1^+(\bar{x}_1,\cdot)\underline{e}_1, \quad (A.5) \\ 0 \le g_1(x_1,\cdot) - \underline{\varphi}_1\left(\bar{x}_1,\underline{x}_1,\cdot\right) \le{}& (\underline{\mathbb{A}}_1 + \bar{\mathbb{A}}_1)(\underline{x}_1,\cdot) \\ & + (\bar{\mathbb{W}}_1^- + \bar{\mathbb{W}}_1^+)(\underline{x}_1,\cdot)\underline{e}_1 + \bar{\mathbb{W}}_1^+(\underline{x}_1,\cdot)\bar{e}_1. \quad (A.6) \end{aligned}$$

It should be pointed out that $(\underline{\mathbb{A}}_1 + \bar{\mathbb{A}}_1)(\bar{x}_1,\cdot)$, $\left(\underline{\mathbb{W}}_1^- + \bar{\mathbb{W}}_1^+\right)(\bar{x}_1,\cdot)$, $\bar{\mathbb{W}}_1^+(\bar{x}_1,\cdot)$ in (*A*.5) are nonnegative, and $(\underline{\mathbb{A}}_1 + \bar{\mathbb{A}}_1)(\underline{x}_1,\cdot)$, $(\bar{\mathbb{W}}_1^- + \bar{\mathbb{W}}_1^+)(\underline{x}_1,\cdot)$, $\bar{\mathbb{W}}_1^+(\underline{x}_1,\cdot)$ in (*A*.6) are also nonnegative.

Remark 12: It is worth pointing out that the continuous function $g_1(x_1, x_2, u)$ may not be local Lipschitz continuous because of the existence of $(\underline{\mathbb{A}}_1 + \bar{\mathbb{A}}_1)(\bar{x}_1,\cdot)$ and $(\underline{\mathbb{A}}_1 + \bar{\mathbb{A}}_1)(\underline{x}_1,\cdot)$ in (*A*.5) and (*A*.6). ∇

References

[1] P. Frank, Fault diagnosis in dynamic systems using analytical and knowledge-based redundancy: A survey and some new results, *Automatica*, vol. 26, no. 3, pp. 459-474, 1990.

[2] J. Chen and R. J. Patton, *Robust model-based fault diagnosis for dynamic systems*, 1st ed. New York, USA: Springer Science & Business Media,1997.

[3] S. Ding, *Model-based fault diagnosis techniques: design schemes, algorithms, and tools*, 1st ed. Heidelberg, Berlin, Genermy: Springer-Verlag, 2008.

[4] K. K. Zhang, B. Jiang, X. G. Yan and Z. H. Mao, Sliding mode observer based incipient sensor fault detection with application to high-speed railway traction device. *ISA transactions*, vol. 69, pp. 49-59, 2016.

[5] S. Yin, H. J. Gao, J. B. Qiu and O. Kaynak. Adaptive fault-tolerant control for nonlinear system with unknown control directions based on fuzzy approximation, *IEEE Transactions on Systems, Man, and Cybernetics: Systems*, vol. 47, no. 8, pp. 1909–1918, 2017.

[6] M. Chen, P. Shi and C. C. Lim, Adaptive neural fault-tolerant control of a 3-DOF model helicopter system, *IEEE Transactions on Systems, Man, and Cybernetics: Systems*, vol. 46, no. 2, pp. 260–270, 2016.

[7] X. D. Zhang, M. M. Polycarpou and T. Parisini, Fault diagnosis of a class of nonlinear uncertain systems with Lipschitz nonlinearities using adaptive estimation, *Automatica*, vol. 46, no. 2, pp. 290–299, 2010.

[8] B. Jiang, M. Staroswiecki and V. Cocquempot, Fault accommodation for nonlinear dynamic systems, *IEEE Transactions on Automatic Control*, vol. 51, no. 9, pp. 1578-1583, 2006.

[9] T. Wang, H. J. Gao, and J. Qiu, A combined fault-tolerant and predictive control for network-based industrial processes, *IEEE Transactions on Industrial Electronics*, vol. 63, no. 4, pp. 2529-2536, 2016.

[10] H. Y. Li, J. H. Wang, H. K. Lam, Q. Zhou, Haiping Du, Adaptive sliding mode control for interval type-2 fuzzy systems, *IEEE Transactions on Systems, Man, and Cybernetics: Systems*, vol. 46, no. 12, pp. 1654-1663, 2016.

[11] H. Zhang, Junmin Wang, Active steering actuator fault detection for an automatically-steered electric ground vehicle, *IEEE Transactions on Vehicular Technology*, vol. 66, no. 5, pp. 3685–3702, 2017.

[12] R. R. Wang, Junmin Wang, Passive actuator fault-tolerant control for a class of overactuated nonlinear systems and applications to electric vehicles, *IEEE Transactions on Vehicular Technology*, vol. 62, no. 3, pp. 972–985, 2013.

[13] R. R. Wang, Junmin Wang, Fault-tolerant control with active fault diagnosis for four-wheel independently driven electric ground vehicles, *IEEE Transactions on Vehicular Technology*, vol. 60, no. 9, pp. 4276–4287, 2011.

[14] Z. H. Zhang and G. H. Yang, Interval observer-based fault isolation for discrete-time fuzzy interconnected systems with unknown interconnections, *IEEE Transactions on Cybernetics*, vol. 47, no. 9, pp. 2413 - 2424, 2017.

[15] J. L. Gouzé, A.Rapaport and M.Z. Hadj-Sadok, Interval observers for uncertain biological systems, *Ecological Modeling*, vol. 133, no. 1, pp. 45-56, 2000.

[16] T. Raïssi, G. Videau and A. Zolghadri, Interval observer design for consistency checks of nonlinear continuous-time systems, *Automatica*, vol. 46, no. 3, pp. 518-527, 2010.

[17] V. Puig, J. Quevedo and T. Escobet, Passive robust fault detection of dynamic processes using interval models, *IEEE Transactions on Control Systems Technology*, vol. 46, no. 3, pp. 1083-1089, 2008.

[18] D. Efimov, L. Fridman and T. Raissi, Interval estimation for LPV systems applying high order sliding mode techniques, *Automatica*, vol. 48, no. 9, pp. 2365-2371, 2012.

[19] M. Moisan and O. Bernard, Robust interval observers for global Lipschitz uncertain chaotic systems, *Systems & Control Letters*, vol. 59, no. 11, pp. 687-694, 2010.

[20] C. Edwards, S.K. Spurgeon and R.J. Patton, Sliding mode observers for fault detection and isolation, *Automatica*, vol. 36, no. 4, pp. 541-553, 2000.

[21] F. J. J. Hermans and M.B. Zarrop, Sliding mode observers for robust sensor monitoring, in *Proceeding of 13th IFAC World Congress*, San Francisco, USA, 1996, pp. 211-216.

[22] W. Chen and W. Saif, Observer-based strategies for actuator fault detection, isolation and estimation for certain class of uncertain nonlinear systems, *IET Control Theory & Applications*, vol. 1, no. 6, pp. 1672-1680, 2007.

[23] K. K. Zhang, B. Jiang, X.G. Yan, J. Shen and Z.H. Mao. Interval sliding mode observer based incipient fault detection with application to a high-speed railway traction device, in *Proceeding of IEEE International Symposium on Robotics and Intelligent Sensors (IRIS)*, Tokyo, Japan, pp. 157-162, 2016.

[24] A. M. Annaswamy, F.P. Skantze and A.P. Loh, Adaptive control of continuous time systems with convex/concave parametrization, *Automatica*, vol. 34, no. 1, pp. 33-49, 1998.

[25] A. P. Loh, A.M. Annaswamy and F.P. Skantze, Adaptation in the presence of a general nonlinear parameterization: An error model approach, *IEEE Transactions on Automatic Control*, vol. 44, no. 9, pp. 1634-1652, 1999.

[26] T. Raïssi and E. Denis, Some recent results on the design and implementation of interval observers for uncertain systems, *Automatisierungstechnik*, vol. 66, no. 3, pp. 213–224, 2018.

[27] S. Chebotarev, D. Efimov, T. Raïssi and A. Zolghadri, Interval observers for continuous-time LPV systems with L_1/L_2 performance, *Automatica*, vol. 58, pp. 82–89, 2015.

[28] M. Saif and Y. Guan, A new approach to robust fault detection and identification, *IEEE Transactions on Aerospace and Electronic Systems*, vol. 29, no. 3, pp. 685-695, 1993.

[29] S. H. Li, J. Yang, W. H. Chen and X. S. Chen, Generalized extended state observer based control for systems with mismatched uncertainties, *IEEE Transactions on Industrial Electronics*, vol. 59, no. 12, pp. 4792–4802, 2012.

[30] X. G. Yan and C. Edwards, Nonlinear robust fault reconstruction and estimation using a sliding mode observer, *Automatica*, vol. 43, no. 9, pp. 1605-1614, 2007.

[31] H. K. Khalil, *Nonlinear systems*, 3rd ed., London, British: Springer-Verlag, 2000.

[32] B. Mohamed and M.A. Rami, A robust estimation approach for uncertain systems with perturbed measurements, *International Journal of Robust and Nonlinear Control*, vol. 26, no. 4, pp. 834-852, 2016.

[33] X. D. Zhang, Sensor bias fault detection and isolation in a class of nonlinear uncertain systems using adaptive estimation, *IEEE Transactions on Automatic Control*, vol. 56, no. 5, pp. 1220-1226, 2011.

[34] K. K. Zhang, B. Jiang, X. G. Yan and Z. H. Mao, Incipient voltage sensor fault isolation for rectifier in railway electrical traction systems, *IEEE Transactions on Industrial Electronics*, vol. 64, no. 8, pp. 6763–6774, 2017.
[35] H. Ziade, R. A. Ayoubi and R. Velazco, A survey on fault injection techniques, *The International Arab Journal of Information Technology*, vol. 1, no. 2, pp. 171–186, 2004.
[36] C. H. Yang, C. Yang, T. Peng, X. Y. Yang and W. H. Gui, A fault-injection strategy for traction drive control systems, *IEEE Transactions on Industrial Electronics*, vol. 64, no. 7, pp. 5719–5727, 2017.
[37] W. Song, X. Feng and C. Xiong, A neutral point voltage regulation method with SVPWM control for single-phase three-level NPC converters, in *Proceeding of IEEE Vehicle Power and Propulsion Conference*, Harbin, China, 2008, pp. 1-4.
[38] A. Abramovitz, An approach to average modeling and simulation of switch-mode systems, *IEEE Transactions on Education*, vol. 54, no. 3, pp. 509-517, 2011.

Kangkang Zhang received the B.Sc. degree in automatic control from Henan University of Technology, Henan, China in 2008, M.Sc. degree in control theory and control engineering from Northeastern University, Shenyang, China in 2014, and PH.D. degree in control theory and control engineering from Nanjing University of Aeronautics and Astronautics (NUAA), Nanjing, China in 2018. He was a visiting Ph.D. student with the University of Kent, United Kingdom in 2017. He is now a Post-Doctoral Fellow in NUAA and a Research Fellow at KIOS Research and Innovation Center of Excellence in Cyprus. His research interests cover fault diagnosis and fault-tolerant control, sliding mode observer and control, interval observer and adaptive estimation and their applications in high-speed trains.

Bin Jiang received the Ph.D. degree in automatic control from Northeastern University, Shenyang, China, in 1995. He had been a Post-Doctoral Fellow, a Research Fellow and a Visiting Professor in Singapore, France, USA, and Canada, respectively. He is currently a Chair Professor of the Cheung Kong Scholar Program, Ministry of Education, and the Dean of College of Automation Engineering, Nanjing University of Aeronautics and Astronautics, China. His research interests include fault diagnosis and fault-tolerant control and their applications in aircraft, satellite and high-speed trains. He is an Associate Editor or Editorial Board Member for a number of journals, such as IEEE TRANSACTION ON CONTROL SYSTEMS TECHNOLOGY, International Journal of Control, Automation and Systems, Nonlinear Analysis, Hybrid Systems, Acta Automatica Sinica, Journal of Astronautics; Control and Decision, and Systems Engineering and Electronics Technologies.

Xing-Gang Yan received the B.Sc. degree from Shaanxi Normal University in 1985, the M.Sc. degree from Qufu Normal University in 1991, and the Ph.D. degree in engineering from Northeastern University, China, in 1997. He was a Lecturer with Qingdao University, China, from 1991 to 1994. He was a Research Fellow/Associate with the University of Hong Kong, China, with Nanyang Technological University, Singapore, and with University of Leicester, U.K. He is currently a Senior Lecturer with University of Kent, U.K. He is the Editor-in-Chief of International Journal of Engineering Research and Science & Technology. His research interests include sliding mode control, decentralised control, fault detection and isolation, and control and observation of nonlinear systems and time delay systems with applications.

Jun Shen received the B.Sc. and M.Sc. degrees from Southeast University, Nanjing, China, in 2008 and 2011, respectively, and the Ph.D. degree from the Department of Mechanical Engineering, the University of Hong Kong, Hong Kong, in 2015. Since 2016 he is an Associate Professor in the College of Automation Engineering, Nanjing University of Aeronautics and Astronautics, Nanjing, China. His current research interests include positive systems, monotone systems, fractional order systems, model reduction, and robust control and filtering.